Supporting Information

Engineering $Cu_{2-x}S$-conjugated upconverting nanocomposites for NIR-II light-induced enhanced chemodynamic/photothermal therapy of cancer

Kaimin Du,[a,b] Shuang Zhao,[a] Jing Feng,*[a,b] Xuan Gao,[a,b] Kai Liu[a,c], Xiaozhen Wang*[d], Manli Zhang[a,b], Yao Li[a,b], Yu Lu[a], and Hongjie Zhang*,[a,b,c]

[a]State Key Laboratory of Rare Earth Resource Utilization, Changchun Institute of Applied Chemistry, Chinese Academy of Sciences, 5625 Renmin Street, Changchun 130022, China
[b]University of Science and Technology of China, Hefei 230026, China
[c]Department of Chemistry, Tsinghua University, Beijing 100084, China
[d]The First Hospital of Jilin University, Changchun 130021, China

*Corresponding authors.
E-mail addresses: fengj@ciac.ac.cn (J. Feng), xzwang@jlu.edu.cn (X. Z. Wang), hongjie@ciac.ac.cn (H. J. Zhang)

Suppporting Figures

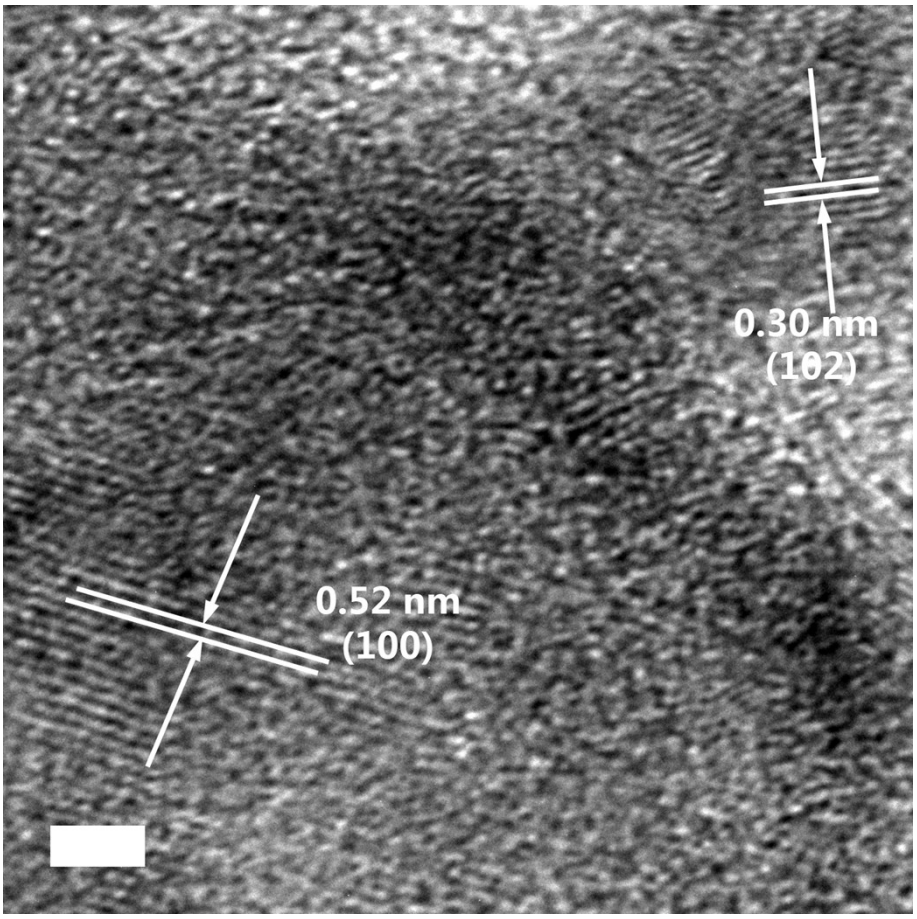

Figure S1. HRTEM image of UCNPs-$Cu_{2-x}S$.

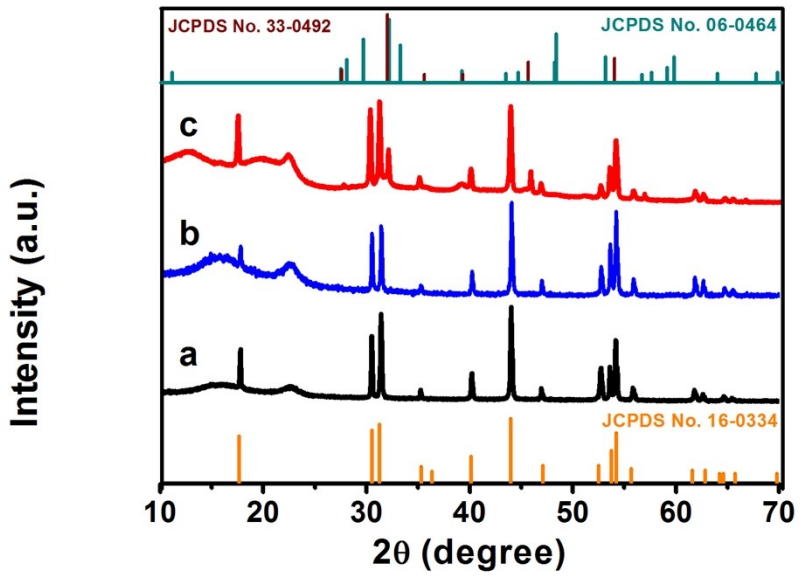

Figure S2. XRD patterns of $NaYF_4$:Yb/Er (black line), $NaYF_4$:Yb/Er@$NaYF_4$:Yb (blue line), and UCNPs-$Cu_{2-x}S$ (red line). The vertical bars show the peak positions and intensities for pure $NaYF_4$ (JCPDS No. 16-0334), Cu_2S (JCPDS No. 33-0492) and CuS (JCPDS card no. 06-0464) as the references.

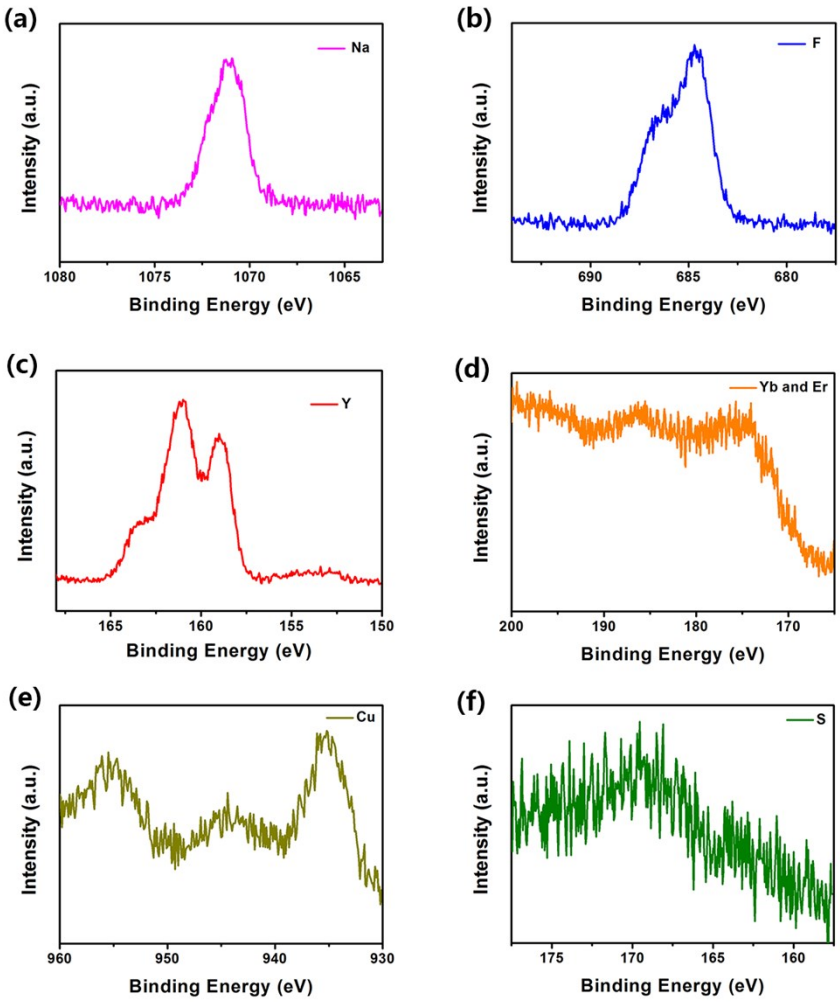

Figure S3. X-ray photoelectron spectroscopy of UCNPs-$Cu_{2-x}S$.

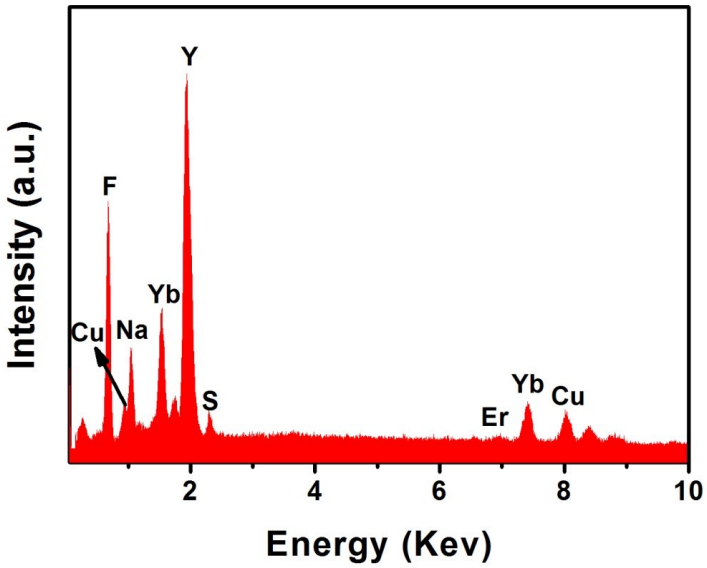

Figure S4. Energy-dispersive X-ray (EDX) spectrum of UCNPs-$Cu_{2-x}S$.

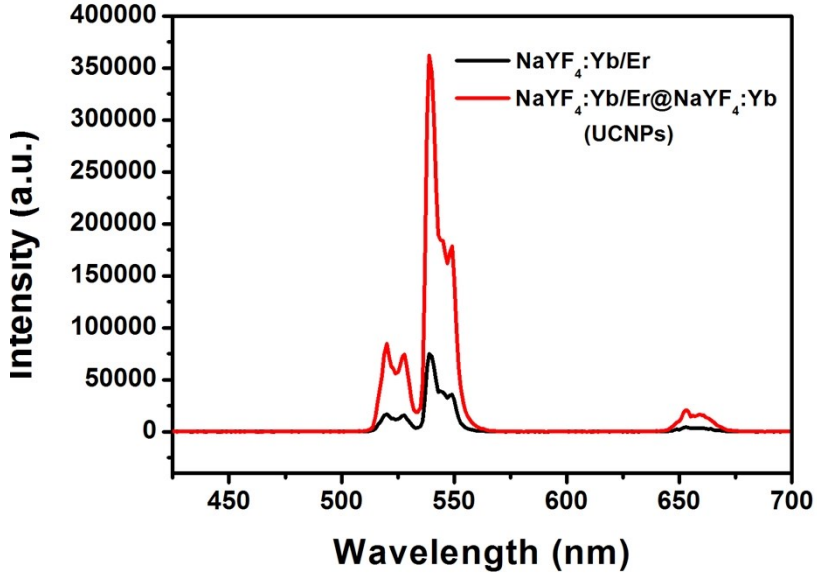

Figure S5. UCL spectra of $NaYF_4$:Yb/Er core and $NaYF_4$:Yb/Er@$NaYF_4$:Yb core-shell nanoparticles in cyclohexane excited by 980-nm NIR laser.

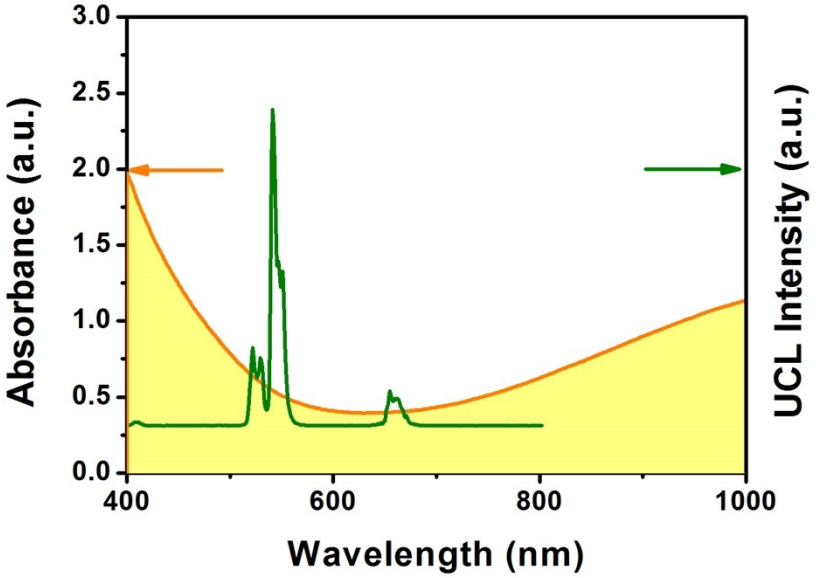

Figure S6. Spectral overlap between the UCL spectrum of CS-UCNPs (red line) and absorption spectrum of UCNPs-$Cu_{2-x}S$ (orange line).

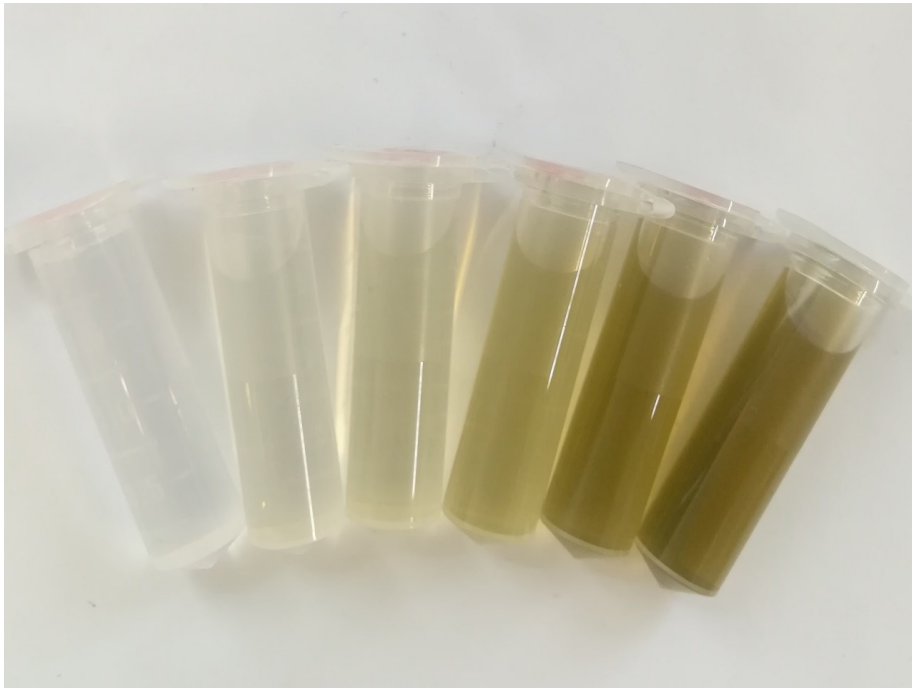

Figure S7. The digital photograph of UCNPs-$Cu_{2-x}S$ solution with different Cu concentrations (0, 12.5, 25, 50, 100 and 200 μg/mL).

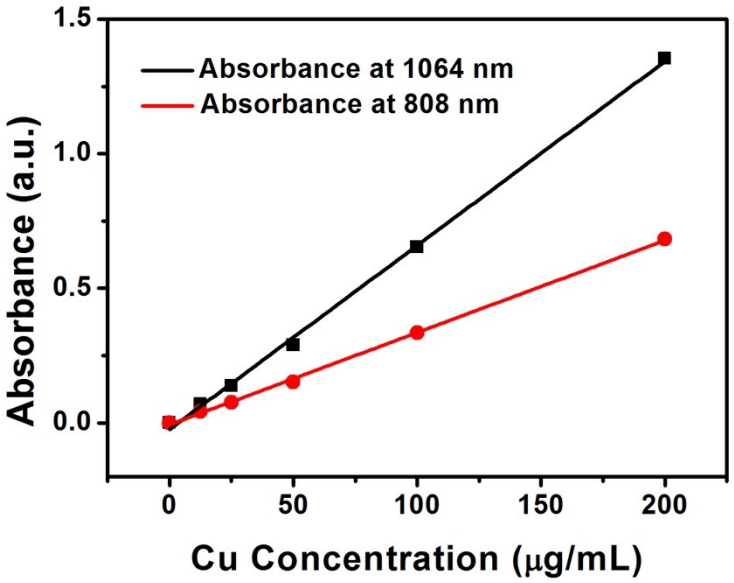

Figure S8. A linear relationship for the optical absorbance at 808 nm and 1064 nm as a function of the concentration of UCNPs-$Cu_{2-x}S$ nanocomposites.

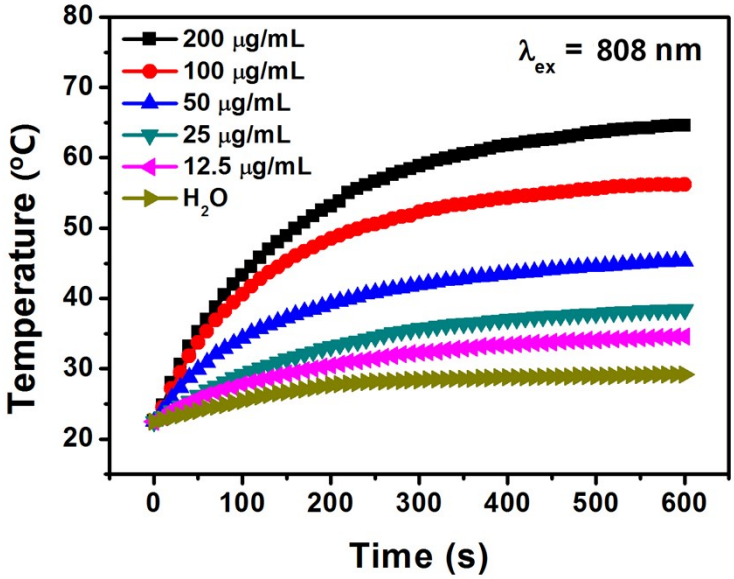

Figure S9. Temperature elevation of water and UCNPs-$Cu_{2-x}S$ aqueous solutions with different concentrations as a function of irradiation time exposure to 808-nm NIR laser (1.0 W/cm^2). The temperature was measured every 10 s using a thermocouple microprobe.

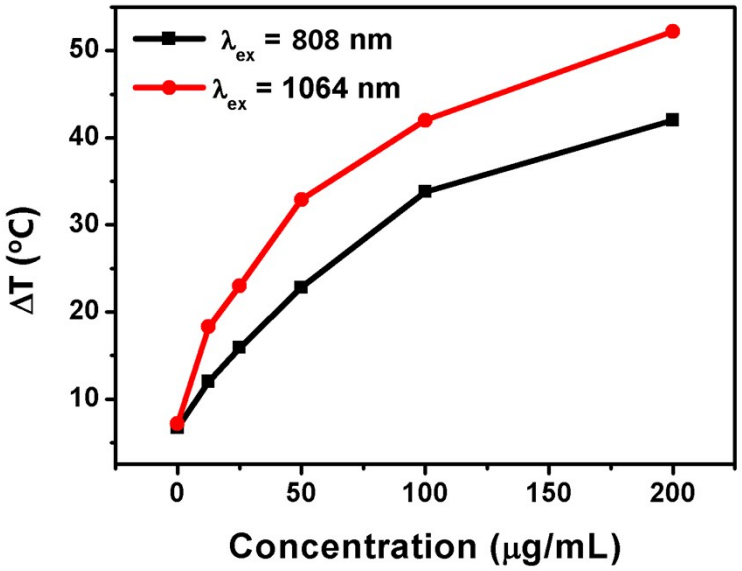

Figure S10. Plot of temperature change (ΔT) over a period of 600 s versus the concentration of UCNPs-$Cu_{2-x}S$ nanocomposites.

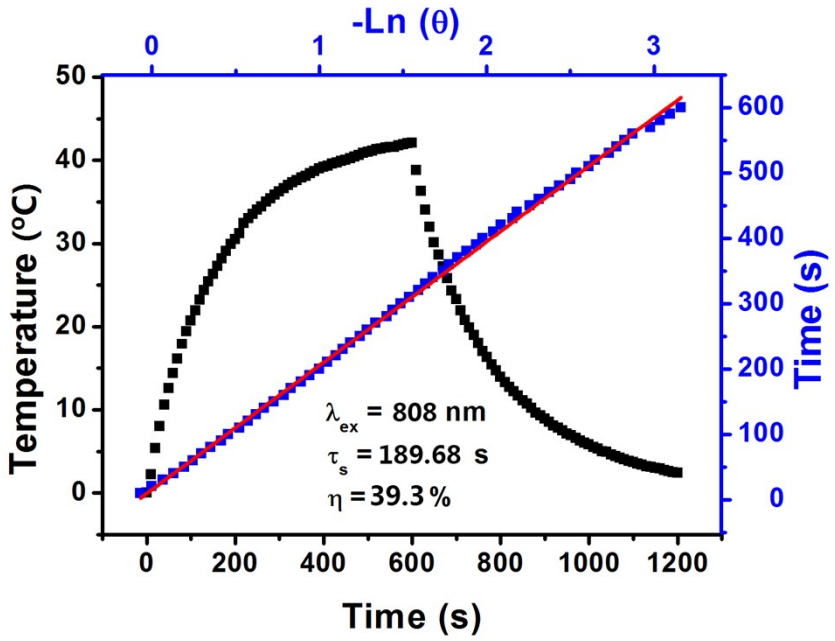

Figure S11. Calculation of the photothermal-conversion efficiency at 808 nm (NIR-I). Black line: The photothermal response of UCNPs-$Cu_{2-x}S$ aqueous solution (200 μg/mL) for 600 s with NIR-I laser and then the laser was shut off. Red line: linear time data versus -lnθ obtained from the cooling period.

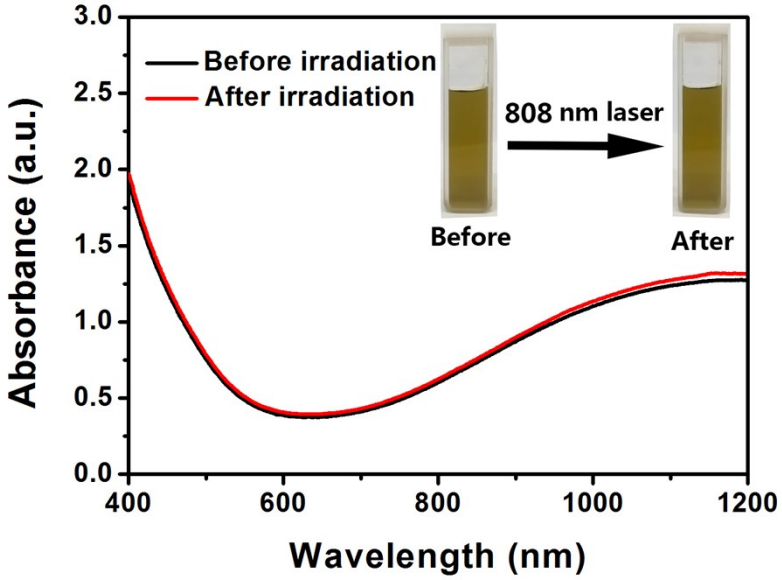

Figure S12. UV-vis–NIR absorption spectra of UCNPs-$Cu_{2-x}S$ dispersion before and after 1 h laser irradiation (808 nm, 1.0 W/cm^2); inset pictures represented the well-dispersed UCNPs-$Cu_{2-x}S$ solution before and after irradiation.

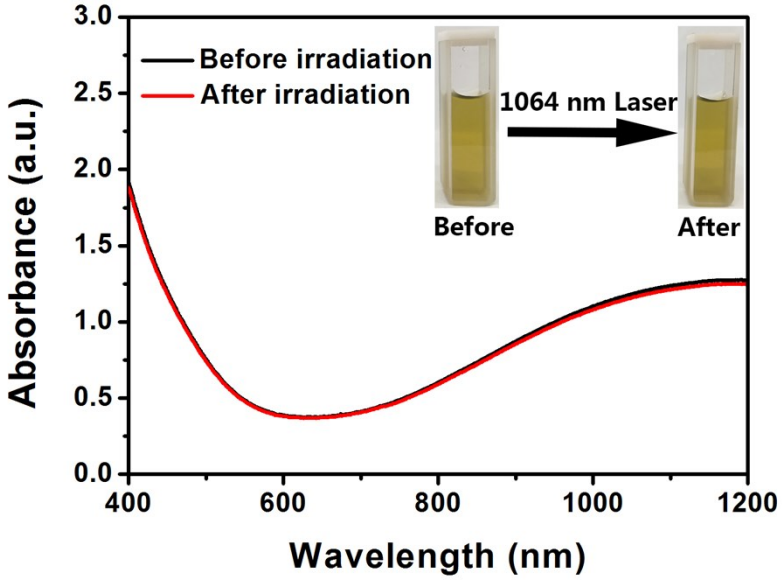

Figure S13. UV-vis–NIR absorption spectra of UCNPs-$Cu_{2-x}S$ dispersion before and after 1 h laser irradiation (1064 nm, 1.0 W/cm^2); inset pictures represented the well-dispersed UCNPs-$Cu_{2-x}S$ solution before and after irradiation.

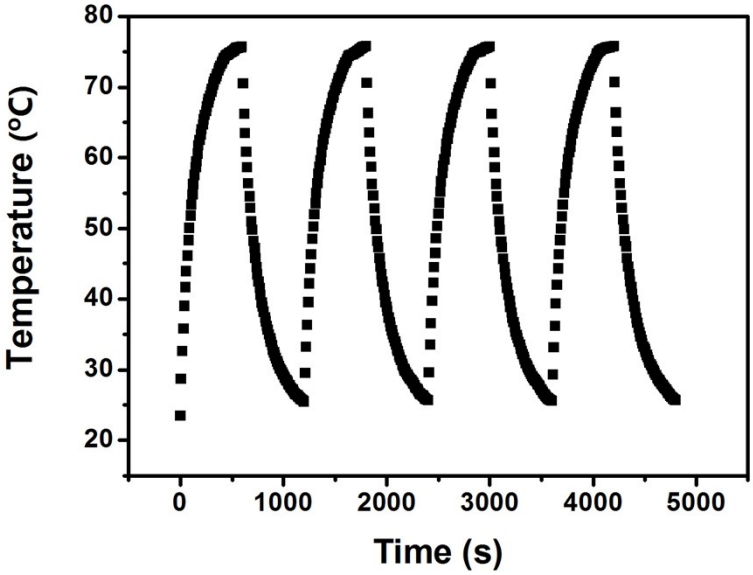

Figure S14. Temperature variation of UCNPs-$Cu_{2-x}S$ aqueous solution (200 μg/mL) under "on-off" cycles of 1064 nm laser irradiation.

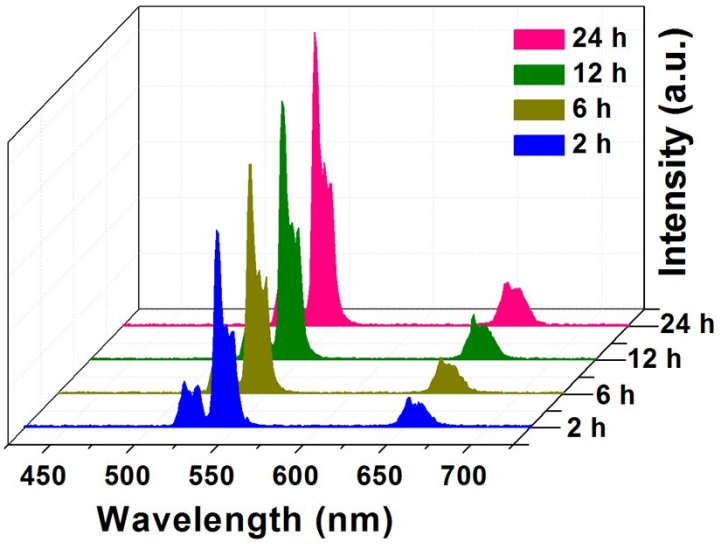

Figure S15. Time-dependent UCL spectra of HeLa cells incubated with UCNPs-$Cu_{2-x}S$ nanocomposites.

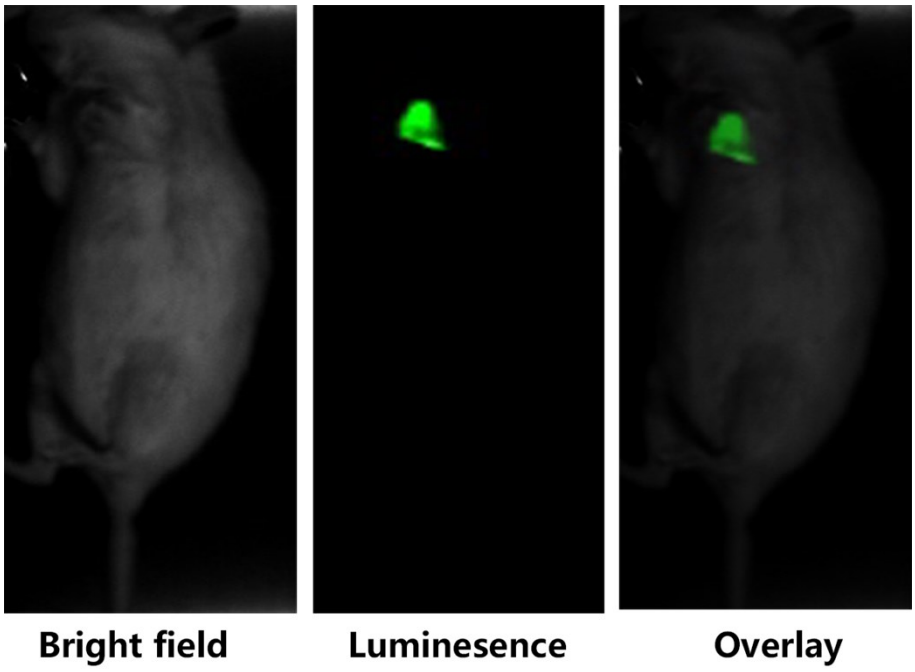

Figure S16. *In vivo* UCL images of the mouse after intratumoral injection of UCNPs-$Cu_{2-x}S$ nanocomposites.

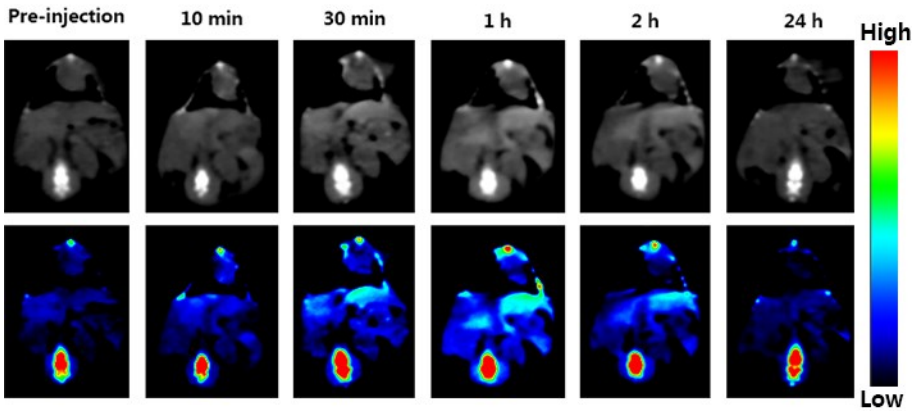

Figure S17. *In vivo* CT coronal view images of a mouse after intravenous injection of UCNPs-$Cu_{2-x}S$ nanocomposites at timed intervals.

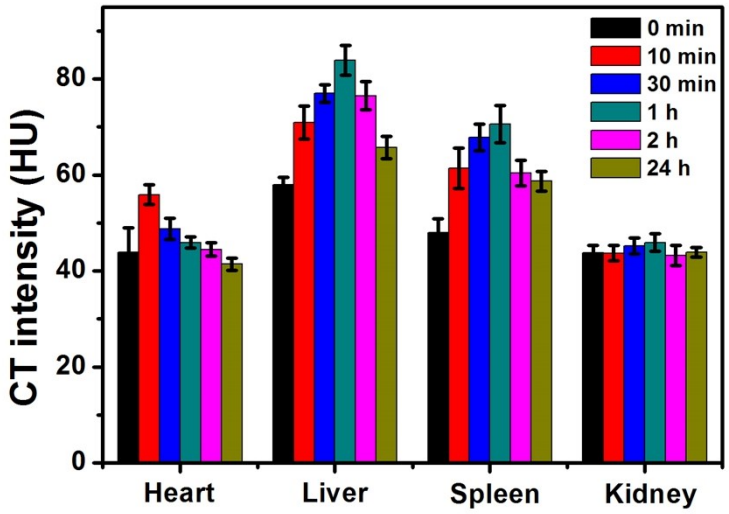

Figure S18. The HU values of different organs of a mouse after intravenous injection of UCNPs-$Cu_{2-x}S$ nanocomposites at timed intervals.